




Sub-ppm acetic acid gas sensor based on In₂O₃ nanofibers

Yu-Chong Wang¹, Zhong-Sen Sun¹, Su-Zhen Wang¹, Shu-Ying Wang¹, Sheng-Xun Cai¹, Xin-Yu Huang¹, Ke Li¹, Zong-Tao Chi^{1,2,*}, Shu-Di Pan^{4,*}, and Wan-Feng Xie^{1,2,3,*} 

¹School of Electronics and Information, Qingdao University, Qingdao 266071, China

²State Key Laboratory of Bio-Fibers and Eco-Textiles, Qingdao University, Qingdao 266071, China

³School of Material Science and Engineering, Qingdao University, Qingdao 266071, China

⁴School of Physics, Qingdao University, Qingdao 266071, China

Received: 28 May 2019

Accepted: 23 July 2019

Published online:

1 August 2019

© Springer Science+Business Media, LLC, part of Springer Nature 2019

ABSTRACT

Metal oxide semiconductor sensors based on nanocrystalline In₂O₃ and its composites are found to be very sensitive in detecting low-concentration (~ 5 ppm) gases such as ozone, nitrogen dioxide, formaldehyde and butane. Here, we successfully obtained fiber-shaped In₂O₃ crystalline nanofibers via electrospun and calcination routes. The gas sensing properties of the In₂O₃ nanofibers were studied by exposing them to the acetic acid vapor with different concentrations from 500 ppb to 2000 ppm at the optimum operating temperature (250 °C). The device possesses ultra-high response of 66.7 toward 2000 ppm acetic acid vapor, low response and recovery times of 25 s and 37 s (100 ppm), respectively, and significant selectivity to acetic acid at 100 ppm. In particular, the sensor based on In₂O₃ nanofibers has very low detection limit and can reach 500 ppb. Therefore, the presented In₂O₃ nanofiber sensor can be used in practice in acetic acid detection area in the future.

Introduction

Acetic acid is colorless, flammable and easy volatile and is extensively used in plastics, pharmaceuticals, dyes, insecticides and photographic chemicals industries [1]. However, inhalation of a certain amount of acetic acid gas can induce irritation in skin, eyes and respiratory system. A long-term exposure in the ambient of acetic acid leakage may induce some kinds of diseases [2, 3]. The maximum permitted

concentrations of acetic acid vapor in workplace are 7.5 ppm in China (GBZ 2-2002) and 9.3 ppm in USA (D3620-04). So, it is very urgent to have a effective way to probe acetic acid concentration in the laboratory and domestic utilities. Unfortunately, the detection toward acetic acid is still unsatisfied [4–8]. For example, the sensing properties, especially sensitivity and working temperature, need to be improved further [1, 4]. In recent decades, gas sensors are highly required in medical, environmental

Address correspondence to E-mail: zoc545s@163.com; psd66zx@163.com; wfxie@qdu.edu.cn

and domestic utilities for detecting toxic and combustible gases. In this respect, metal oxide semiconductors (MOSCs) such as ZnO [1], Bi₂O₃ [9], SnO₂ [8, 10], α -Fe₂O₃ [7], MoO₃ [11], In₂O₃ [12–15] and their nanocomposites are promising candidates owing to their thermal stability, excellent response, reversibility and effective cost [16, 17]. In order to increase sensitivity and decrease operating temperature of the gas sensor, noble metals and transition metals are favorite dopants, which can significantly enhance the sensing properties of MOSCs [18–21]. But, these types of sensors have the disadvantages of complicated synthesis process, narrow range of detection limit and high working temperature [19, 20]. The sensors based on semiconductor oxides can work via the variation in the device resistance due to the surface processes of sensing materials [18, 19]. In general, the absorbed acetic acid gas molecule could decompose into two CO₂, two H₂O molecules and eight electrons ($8 e^{-}$) due to the lower bond energy of C–C in CH₃COOH, and then the released electrons result in an abrupt alteration of device's resistance [2, 3, 18].

In a wide variety of MOSC nanomaterials, In₂O₃ and its composites exhibit higher sensitivity and shorter response/recovery times than other sensing materials [9, 22]. For example, the sensing performance of Bi₂O₃-decorated In₂O₃ nanorods is stronger (1.5–4.9 times) than that of the pristine In₂O₃ nanorod at the corresponding concentrations [9]. And the nanosheet-based In₂O₃ microflowers gas sensor exhibited excellent sensing properties toward formaldehyde [22]. In 2018, the broken In₂O₃ microtubes were obtained by chemical conversion method, and these broken In₂O₃ microtubes exhibited significant response toward triethylamine at 1–100 ppm, and the detection limit is 0.1 ppm [23]. Very recently, Co-doped In₂O₃ nanorods were fabricated by hydrothermal strategy, and the In₂O₃/1%Co nanorods exhibited a high response of 23.2 for 10 ppm to HCHO at 130 °C [24]. Lee et al. reported that the CuO-loaded In₂O₃ nanofibers significantly enhanced the gas response toward 5 ppm H₂S from 515 to 1.16×10^5 at 150 °C [25]. What's more, one-dimensional (1D) structure allows efficient electron transport along the longitudinal direction, is simple and has high volume prepared by electrospinning [25]. To the best of our knowledge, electrospinning can be used to prepare nanofibers with many particles, which can greatly increase the specific surface area [3, 7, 26]. Up to now, few studies have been reported

regarding the acetic acid sensing characteristics of In₂O₃ nanofibers. Therefore, it is of great significance to design and fabricate an acetic acid sensor with good performance based on In₂O₃ nanofibers.

We have successfully obtained In₂O₃ nanofibers composed of many nanoparticles. The detection limit of In₂O₃ nanofibers sensor can reach 500 ppb and has excellent selectivity toward acetic acid. Meanwhile, the homemade devices exhibit good repeatability and stability.

Experimental section

Materials

Polyvinylpyrrolidone (PVP, $M_w = 1500000$), indium(III) nitrate hydrate (In(NO₃)₃·H₂O) and *N,N*-dimethylformamide (DMF) were purchased from Aladdin Company and used without any purification.

Preparation of In₂O₃ nanofibers

In this study, the In₂O₃ nanofibers were fabricated via electrospinning combined with calcination in air. Typically, 0.5 g of In(NO₃)₃·H₂O was added into a solvent of DMF in a little bottle under vigorous stirring for 6 h. Then, 0.25 g of PVP was dissolved into 3 ml ethanol in another little bottle under vigorous stirring for 6 h. Then, both of them were mixed together under stirring and loaded into a 10-ml injector with a 22-gauge needle tip for electrospinning, and the parameters of electrospinning are the same as the above process. After electrospinning, the nanofiber-shaped In₂O₃ precursors were preheated at 160 °C for 2 h and then calcined at 600 °C under air for 4 h. Finally, the In₂O₃ nanofibers composed of many nanoparticles were successfully obtained.

Characterizations

The surface morphology of the nanofibers was observed using a field emission scanning electron microscope (FESEM, Zeiss Gemini 500). The diameter of the electrospun fibers was measured using image analysis software (Adobe Acrobat X Pro 10.1.2.45) according to the SEM images. Energy-dispersive X-ray spectroscopy (EDX) mapping of the samples was performed using an Oxford Link-ISIS 300 EDX

attachment at 15 kV. The microstructure of the samples was investigated by X-ray diffraction (XRD), performed on a Bruker D8 diffractometer with Cu K α radiation ($\lambda = 0.154$ nm). XPS measurements were recorded with a Thermo Scientific Escalab 250xi instrument equipped with a monochromatic Al K α source. And the gas sensing properties were measured by WS-30A gas sensing measurement system. During the tests of gas sensing, a certain volume of the acetic acid liquid was injected into the test chamber. When the resistance of the sensor was stable, the sensor was transferred into another chamber that was full of fresh air and began to recover. The testing chamber was blown and purged by nitrogen (purity: 99.9%) before and after every cycle. In this article, the sensor response to the testing gas is defined as $R = R_a/R_g$, where R_a and R_g are the resistances of the sensors in air and in target gases, respectively. Here, the response/recovery times were defined as the time taken to achieve 90% of the total

resistance changes after the sensor was exposed to the acetic acid vapor and fresh air, respectively.

Results and discussion

Figure 1a illustrates an overall process of material synthesis and device preparation. Here, we firstly obtained In₂O₃ nanofibers via electrospinning and calcination routes, and then the sensing devices based on In₂O₃ nanofibers were prepared according to our previous report [27]. In Fig. 1b, it can be seen that the In₂O₃ precursors formed a multilayered network randomly, which is similar to a nonwoven nanofiber mat (inset in Fig. 1b). As depicted in the high-magnitude SEM in Fig. 1c, the as-prepared In₂O₃ precursors have uniform shape and smooth surface, without any obvious beads and defects on the surface of the precursors, which implies that the In₂O₃ electrospinning solution has good spinnability

Figure 1 a Schematic illustration of the fabrication processes for In₂O₃ nanofibers and corresponding gas sensor. b The SEM image of In₂O₃ precursor fibers; the inset is nonwoven In₂O₃ nanofiber mat. c High-resolution SEM image of In₂O₃ precursor fibers, and the inset is histograms of the corresponding In₂O₃ precursor diameters. d Low-magnitude SEM image of the calcined In₂O₃ nanofibers. e High-resolution SEM image of In₂O₃ nanofibers, and the inset is histograms of the corresponding In₂O₃ nanofibers diameters.

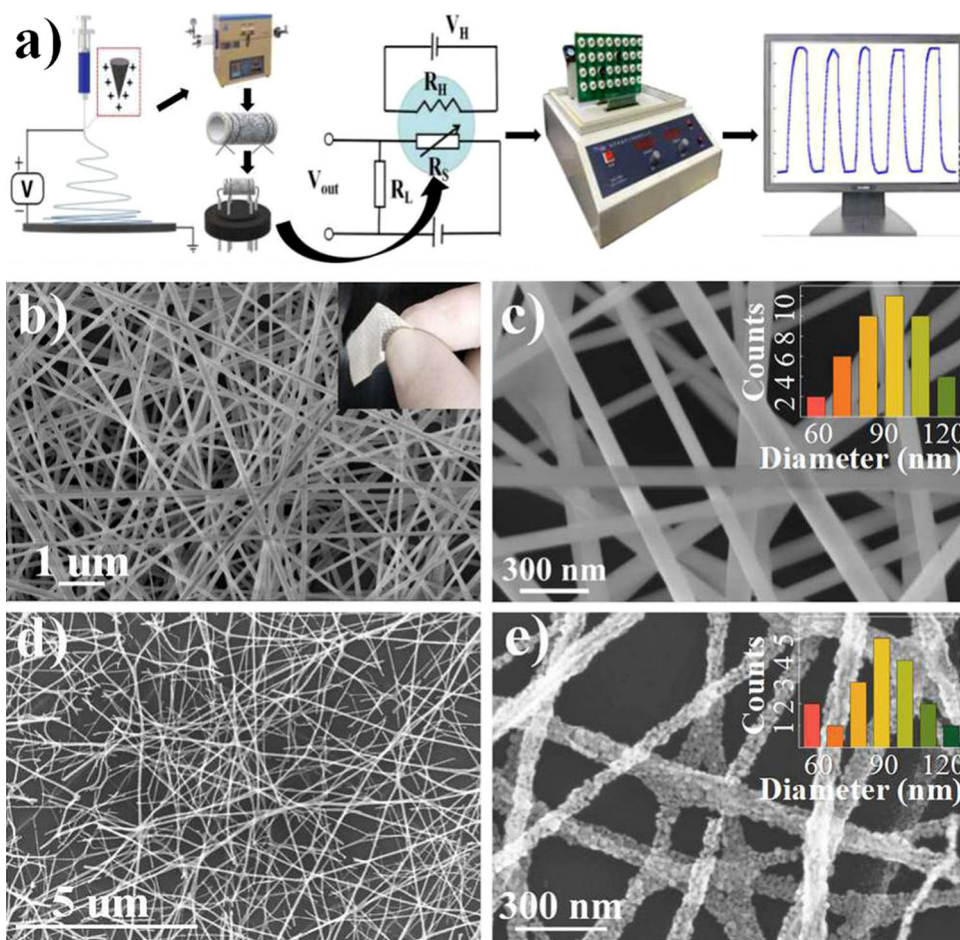
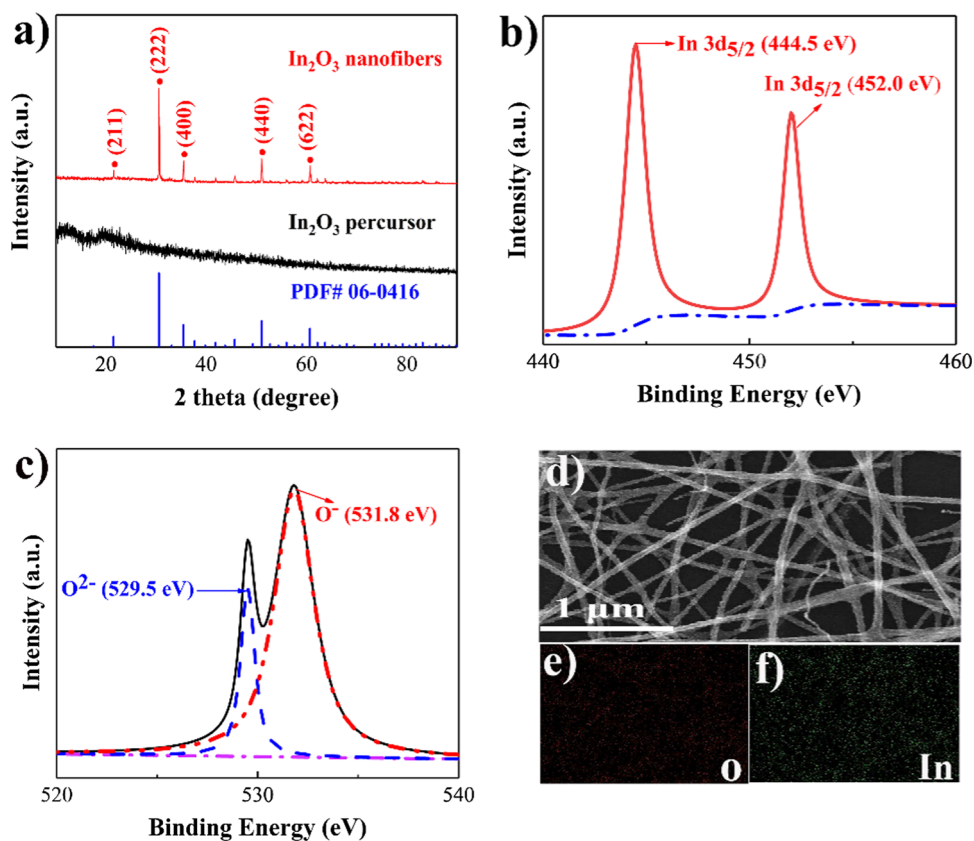


Figure 2 **a** XRD pattern of In_2O_3 /PVP composite fibers (In_2O_3 precursor fibers) and In_2O_3 nanofibers, respectively. **b** and **c** are high-resolution XPS spectra of In 3d and O 1s of In_2O_3 nanofibers, respectively. **d**, **e** and **f** are the corresponding energy-dispersive X-ray spectroscopic (EDX) elemental mapping images of O **e** and In **f**, respectively.



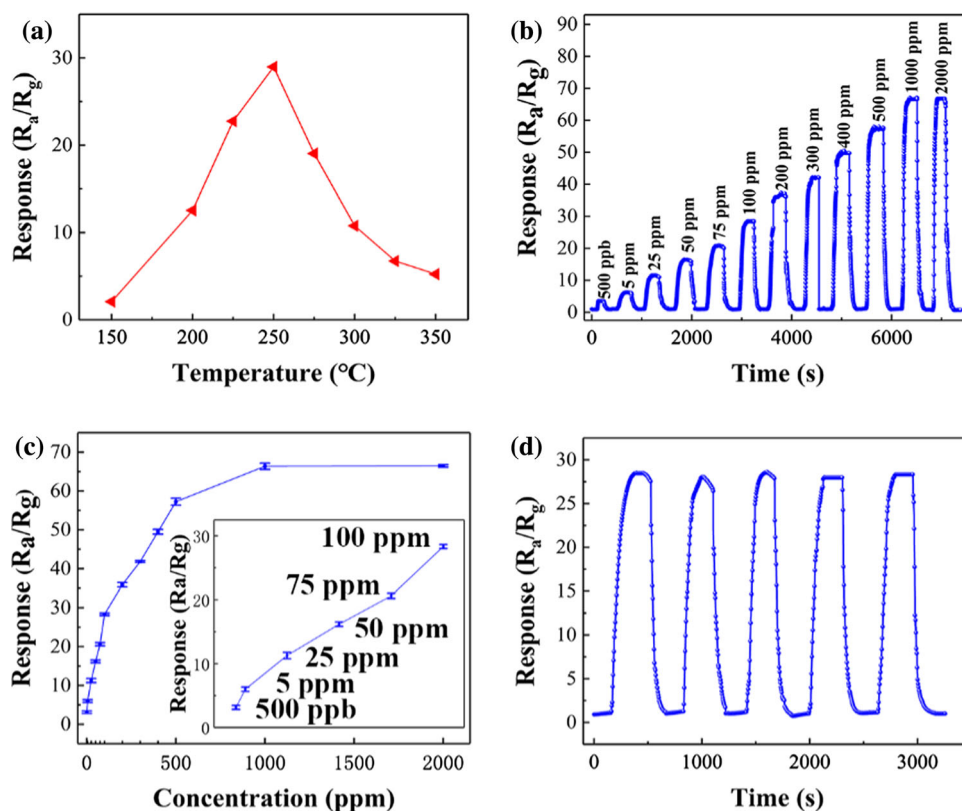
[28, 29]; see Fig. 1c. In addition, the diameter of the In_2O_3 precursors is roughly distributed at 90 nm, as shown in the inset of Fig. 1c. Then, the In_2O_3 precursors were calcined in air at 600 °C immediately after preheating at 160 °C. The In_2O_3 precursors were broken into pieces after calcination process; see Fig. 1d (the low-magnitude SEM image). In order to investigate the details of the calcined In_2O_3 nanofibers, the high-resolution SEM image was taken (Fig. 1e). Evidently, it can be seen that the surface of the In_2O_3 nanofibers are uneven, compared to the In_2O_3 precursors. Besides, some nanoparticles appeared on the surface of In_2O_3 nanofibers. Such structure plays a significant role in gas sensing enhancement because the rough surface can greatly increase the active sites to the target gas. On the other hand, the roughened surface is benefit to gas adsorption/desorption and diffusion of target gas molecule [22, 27]. Additionally, the diameter tendency observed in the as-spun nanofibers was decreased after calcination [7, 29]. According to the statistical result, the average diameter of In_2O_3 nanofibers (the inset of Fig. 1e) decreased by approximately 22% compared to the distribution of

In_2O_3 precursors (see the inset of Fig. 1c). This obvious decrease in diameter was attributed to either the evaporation of residual solvent (DMF) absorbed in the fibers or a partial decomposition of PVP, which acts as the polymeric scaffold of In_2O_3 precursors [29].

To investigate the purity and crystalline phases of the samples, the XRD patterns of In_2O_3 precursors and In_2O_3 nanofibers were scanned from 10° to 90°. Obviously, the XRD pattern of In_2O_3 precursors (stabilized at 160 °C) did not reveal any crystalline structure (Fig. 2a, dark pattern). In contrast, the calcined In_2O_3 nanofibers exhibit strong diffraction peaks, as shown in Fig. 2a (red pattern). It can be observed that the peaks of crystal planes (211), (222), (400), (440) and (622) are the main characteristic peaks of In_2O_3 , which correspond to cubic structure of In_2O_3 (JCPDS 06-0416) [28, 30]. The result suggests that In_2O_3 nanofibers with excellent crystallinity were successfully synthesized [30].

The high-resolution XPS measurement was carried out to analyze the chemical constituents and elements valence of the In_2O_3 nanofibers. Figure 2b shows the XPS spectrum of In 3d state, which indicates the

Figure 3 **a** Sensing performances of the In_2O_3 nanoparticle fibers toward 100 ppm acetic acid gas at different operating temperatures. **b** Dynamic response curves of the In_2O_3 sensor toward acetic acid from 500 ppb to 2000 ppm at 250 °C. **c** Response versus gas concentrations for In_2O_3 sensors, and the inset gives the curve of low concentration from 500 ppb to 100 ppm. **d** Repeatability test (five periods) of the In_2O_3 nanoparticle fibers sensor to 100 ppm of acetic acid at 250 °C.



peaks at 444.5 eV and 452.0 eV, corresponding to the $\text{In } 3d_{5/2}$ and $\text{In } 3d_{3/2}$, respectively. The difference value between $\text{In } 3d_{3/2}$ and $\text{In } 3d_{5/2}$ is 7.5 eV, which indicates that In element exists mainly in the state of In^{3+} in In_2O_3 [23, 24, 28]. Figure 2c shows two peaks of the oxygen species and the lower energy peak (529.5 eV) can be attributed to lattice oxygen on the surface of In_2O_3 nanofibers, while the peak located at 531.8 eV may be ascribed to chemisorbed oxygen species. According to the previous reports, the chemisorbed oxygen is good for catalytic activity in gas sensors and to improve the performance of volatile organic compound (VOC) gas sensors [7, 18]. Besides, the elemental mapping images (Fig. 2d–f) further confirmed the composition of the product and the spatial distribution of the elements. Obviously, O (Fig. 2e) and In (Fig. 2f) signals were detected as a fiber-like structure, while In and O signals were detected in the whole region, which indicated the uniform distributions of In and O elements over the whole nanofibers.

In order to ascertain the optimum operating temperature of the In_2O_3 nanofibers sensor, the response value of the sensor toward 100 ppm acetic acid under different temperatures from 150 to 350 °C was

measured and the results are shown in Fig. 3a. We can see that the response increases sharply with the increase in temperature from 150 to 250 °C for the In_2O_3 nanofibers sensor and reaches the maximum value of 28.4 at 250 °C, and then drops rapidly with further increase in the temperature.

Above the temperature of 250 °C, the decrease in adsorbed oxygen ions will increase conduction electron density and thus reduce the gas response. Therefore, the optimum working temperature should be 250 °C to proceed with the following measurements. Figure 3b gives the dynamic response and recovery properties of sensors based on In_2O_3 nanofibers of different acetic acid vapor concentrations (from 500 ppb to 2000 ppm) at 250 °C. We can see that the response increases quickly with the increase in the acetic acid concentration; see Fig. 3c, and the response of the In_2O_3 nanofibers sensor increases steeply from 500 ppb to 100 ppm (inset in Fig. 3c). Thus, the In_2O_3 nanofibers sensor can effectively detect acetic acid with the ultra-low concentration due to the nature of one-dimensional (1D) structures, which can facilitate the rapid and efficient adsorption of gas molecules, as well as good sensing performance. It is worth mentioning that the response is 3.4

Table 1 Response values of In_2O_3 nanofiber sensor at different concentrations of acetic acid from 500 ppb to 2000 ppm

Concentration	500 ppb	5 ppm	25 ppm	50 ppm	75 ppm	100 ppm
Response	3.4	6.22	11.5	16.4	20.9	28.4
Concentration	200 ppm	300 ppm	400 ppm	500 ppm	1000 ppm	2000 ppm
Response	36.5	42.0	49.7	57.2	66.6	66.7

at 500 ppb, which is larger than that of international criterion of 1.2 [19, 20]. The lower limit of quantitation (LLOQ) of acetic acid vapor is evaluated by linear extrapolation of the response sensitivity as a function of acetic acid concentration, and the calculating formula of the LLOQ is $\text{LLOQ} = 3 \times (\text{standard Deviation/slope})$ [31], predicting an ultra-low acetic acid detection concentration of 161 ppb for the In_2O_3 nanofibers sensor operated at 250 °C. The detailed response values of In_2O_3 nanofiber sensors are listed in Table 1.

When the concentration of acetic acid reaches 1000 ppm, the response value shows the status of saturation and the similar characteristics of other-category VOC sensors have been reported previously [18, 26, 30]. We suggest that the response of gas sensor is determined by the surface reaction rate. Therefore, the large specific surface area is a very

important factor to promote the surface reaction rate [32–34]. According to Table 1, the maximum response value is 66.7 under 2000 ppm, which is very close to 1000 ppm (66.6). On this aspect, the nanoparticles of In_2O_3 nanofibers greatly affect the response value of In_2O_3 nanofibers sensor. Figure 3d shows a typical cycling stability test of the In_2O_3 sensor to 100 ppm of acetic acid at 250 °C. It can be found that the In_2O_3 sensor has a consistent response property, and the value is 28.1. In addition, the device exhibits excellent recovery characteristics and repeatability.

Figure 4a gives the response time (τ_{res}) and recovery time (τ_{recov}) of the In_2O_3 nanofibers sensor to 100 ppm acetic acid at 250 °C, which are the vital performance parameters for gas sensors. The τ_{res} of pure In_2O_3 sensor is 25 s, and the measured recovery time (τ_{recov}) is 37 s, which are shorter than those from

Figure 4 a Response and recovery characteristics of the In_2O_3 nanoparticle fibers sensor toward 100 ppm acetic acid at 250 °C. b Line chart of the long-term stability of In_2O_3 sensor of 1 day, 15 days, 30 days, 45 days and 60 days, respectively. c Selectivity of the In_2O_3 nanoparticle fibers sensor toward different VOCs at 250 °C. d Schematic diagram of the acetic acid sensing mechanism of In_2O_3 nanoparticle fibers.

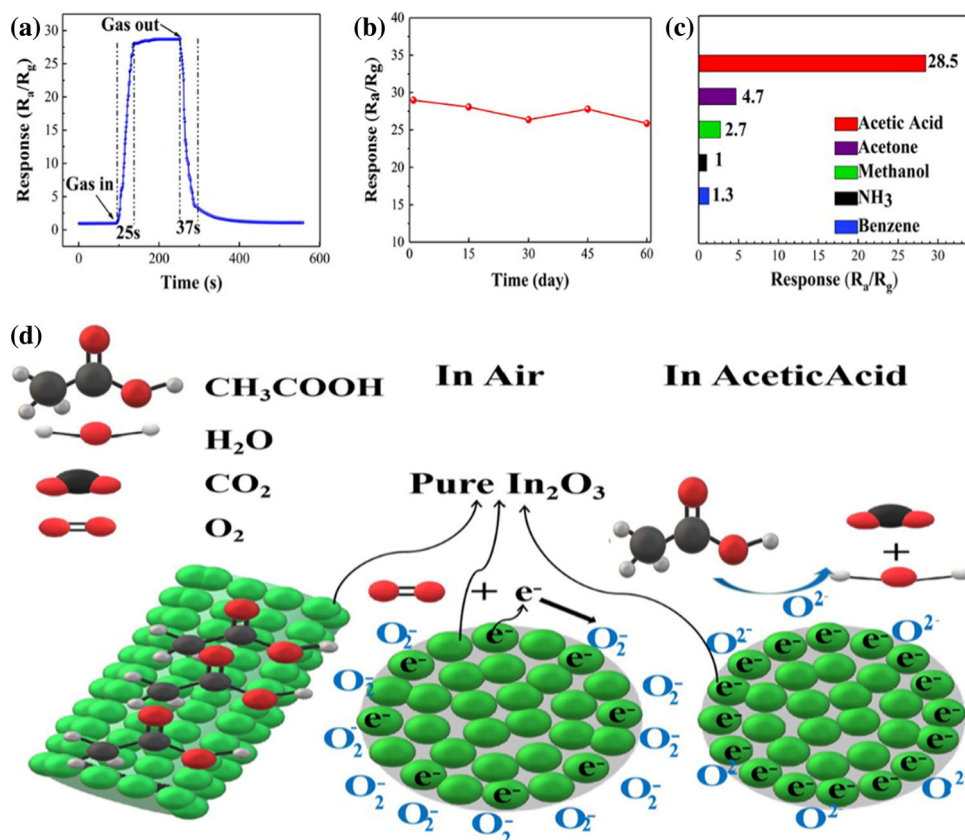


Table 2 Comparison of sensing performance toward acetic acid reported by other groups

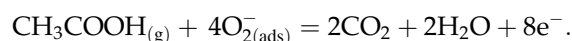
Materials	Concentration (ppm)	T (°C)	R_s	τ_{res} (s)	τ_{recov} (s)	Refs.
CdS _x Se _{1-x} nanoribbons	400	210	6	80	50	[35]
Y-doped SnO ₂ nanoparticles	800	300	300			[4]
Pr-doped ZnO nanofibers	400	380	7.38	51	40	[1]
SnO ₂ nanoflowers	100	260	47.7	18	11	[8]
In ₂ O ₃ nanofibers	100	250	28.4	25	37	This work

previous reports [1–4, 7, 8]. The above results are sufficient to prove that the response and recovery times toward acetic acid gas can be greatly improved by In₂O₃ nanofibers. The long-term stability of In₂O₃ nanofibers gas sensor is also investigated and shown in Fig. 4b. The sensor exhibits nearly constant sensor signals to 100 ppm acetic acid for 60 days, confirming the good stability of the In₂O₃ nanofibers sensor. Again, acetone, methanol, NH₃ and benzene sensing characteristics of the In₂O₃ nanofibers sensors are also measured under the same conditions to evaluate the selectivity of In₂O₃ nanofibers sensor. Figure 4c shows the sensitivities of In₂O₃ nanofibers sensor to 100 ppm of different gases at 250 °C. We can see that In₂O₃ nanofibers sensor show less sensitivity to other gases, indicating the excellent selectivity to acetic acid vapor.

The comparison of the responses to acetic acid gas among the In₂O₃ nanofibers sensors and previous reports such as CdS_xSe_{1-x} nanoribbons, Y-doped SnO₂ nanoparticles, Pr-doped ZnO nanofibers, and SnO₂ nanoflowers is shown in Table 2. In contrast to other materials, the In₂O₃ nanofibers gas sensor has a lower operation temperature and extremely high sensitivity. In short, the In₂O₃ nanofibers gas sensors showed good sensing properties, especially sensitivity and working temperature.

The gas sensing mechanism can be explained as follows: The gas-sensitive materials react with reducing gas such as acetic acid and lead to the change in electrical resistance of the materials, as shown in Fig. 4d [36, 37]. When gas sensors are exposed to air, oxygen molecules are adhered to the surface of In₂O₃ nanofibers and electrons transport occurs between these metal oxides and the gas molecules, leading to the formation of adsorbed oxygen O⁻, O²⁻ and O₂⁻ in the following fashions: O_{2(gas)} + 2e⁻ → 2O_(ads)⁻, O_{2(gas)} + e⁻ → O_{2(ads)}⁻, O_{2(gas)} + e⁻ → O_{2(ads)}⁻ [38–41]. As a result, the carrier concentration will decrease, which results in the increase in

the device resistance. When the sensor is exposed to acetic acid gas, the acetic acid molecules will react with oxygen ions and release a certain number of electrons, which go back to the conduction band, resulting in the resistance decrease of the device. According to the previous reports, the surface process of charge was greatly influenced by surface defect [32]. Hence, the reaction is:



Therefore, the acetic acid sensitivity toward In₂O₃ gas sensors is basically above oxidation reaction process, with free electrons flowing into the conduction band. These free electrons will in turn improve the oxygen adsorption on the In₂O₃ surface [29, 42].

Conclusion

In summary, we have successfully obtained In₂O₃ nanofibers via a synergetic approach of electrospinning and calcination processes. The In₂O₃ nanofibers exhibit enhanced sensing performance toward acetic acid at 250 °C. Specifically, the sensor based on In₂O₃ nanofibers has very low detection limit and can reach 500 ppb. According to our study, it is believed that the sensor based on In₂O₃ nanofibers is a promising candidate for the efficient detection of acetic acid.

Acknowledgements

The authors acknowledge the National Natural Science Foundation of China (Grant No. 51227804), the Natural Science Foundation of Jiangsu Province (BK20170330) and the Postdoctoral Scientific Research Foundation of Qingdao. The authors would also like to thank Chemical Experimental Teaching Center of Qingdao University for the measurement help.

References

- [1] Wang C, Ma S, Sun A, Qin R, Yang F, Li X, Li F, Yang X (2014) Characterization of electrospun Pr-doped ZnO nanostructure for acetic acid sensor. *Sens Actuators B: Chem* 193:326–333
- [2] Bhamore JR, Ganguly P, Kailasa SK (2016) Molecular assembly of 3-mercaptopropionic acid and guanidine acetic acid on silver nanoparticles for selective colorimetric detection of triazophos in water and food samples. *Sens Actuators B: Chem* 233:486–495
- [3] Dedecker K, Pillai RS, Nouar F, Pires J, Steunou N, Dumas E, Maurin G, Serre C, Pinto ML (2018) Metal-organic frameworks for cultural heritage preservation: the case of acetic acid removal. *ACS Appl Mater Interfaces* 10:13886–13894
- [4] Cheng L, Ma SY, Wang TT, Luo J, Li XB, Li WQ, Mao YZ, Gz DJ (2014) Highly sensitive acetic acid gas sensor based on coral-like and Y-doped SnO₂ nanoparticles prepared by electrospinning. *Mater Lett* 137:265–268
- [5] Li XB, Zhang QQ, Ma SY, Wan GX, Li FM, Xu XL (2014) Microstructure optimization and gas sensing improvement of ZnO spherical structure through yttrium doping. *Sens Actuators B: Chem* 195:526–533
- [6] Lin S, Swager TM (2018) Carbon nanotube formic acid sensors using a nickel bis(ortho-diiminoquinonate) selector. *ACS Sens* 3(3):569–573
- [7] Ma L, Ma SY, Qiang Z, Xu XL, Chen Q, Yang HM, Chen H, Ge Q, Zeng QZ, Wang BQ (2017) Preparation of Co-doped LaFeO₃ nanofibers with enhanced acetic acid sensing properties. *Mater Lett* 200:47–50
- [8] Jin WX, Ma SY, Tie ZZ, Li WQ, Luo J, Cheng L, Xu XL, Wang TT, Jiang XH, Mao YZ (2015) Synthesis of hierarchical SnO₂ nanoflowers with enhanced acetic acid gas sensing properties. *Appl Surf Sci* 353:71–78
- [9] Park S, Kim S, Sun GJ, Lee C (2015) Synthesis, structure, and ethanol gas sensing properties of In₂O₃ nanorods decorated with Bi₂O₃ nanoparticles. *ACS Appl Mater Interfaces* 7:38–46
- [10] Wang D, Tian L, Li HJ, Wan KC, Yu X, Wang P, Chen AY, Wang XY, Yang JH (2019) Mesoporous ultrathin SnO₂ nanosheets in situ modified by graphene oxide for extraordinary formaldehyde detection at low temperatures. *ACS Appl Mater Interfaces* 11:12808–12818
- [11] Tian J, Zhang H, Li Z (2018) Synthesis of double-layer nitrogen-doped microporous hollow carbon@MoS₂/MoO₂ nanospheres for supercapacitors. *ACS Appl Mater Interfaces* 10:29511–29520
- [12] Yan SN, Li ZJ, Li H, Wu ZL, Wang JQ, Shen WZ, Fu YQ (2018) Ultra-sensitive room-temperature H₂S sensor using Ag–In₂O₃ nanorod composites. *J Mater Sci* 53:16331–16344. <https://doi.org/10.1007/s10853-018-2789-z>
- [13] Li ZJ, Yan SN, Wu ZL, Li H, Wang JQ, Shen WZ, Wang ZG, Fu YQ (2018) Hydrogen gas sensor based on mesoporous In₂O₃ with fast response/recovery and ppb level detection limit. *Int J Hydrog Energy* 43:22746–22755
- [14] Haiduk YS, Khort AA, Lapchuk NM, Savitsky AA (2019) Study of WO₃–In₂O₃ nanocomposites for highly sensitive CO and NO₂ gas sensors. *J Solid State Chem* 273:25–31
- [15] Lee CS, Li HY, Kim BY, Jo YM, Byun HG, Hwang IS, Abdel-Hady F, Wazzan AA, Lee JH (2019) Discriminative detection of indoor volatile organic compounds using a sensor array based on pure and Fe-doped In₂O₃ nanofibers. *Sens Actuators B: Chem* 285:193–200
- [16] Xu S, Xu Y, Zhao H, Xu R, Lei Y (2018) Sensitive gas-sensing by creating adsorption active sites: coating an SnO₂ layer on triangle arrays. *ACS Appl Mater Interfaces* 10:29092–29099
- [17] Dong C, Liu X, Han B, Deng S, Xiao X, Wang Y (2016) Nonaqueous synthesis of Ag-functionalized In₂O₃/ZnO nanocomposites for highly sensitive formaldehyde sensor. *Sens Actuators B: Chem* 224:193–200
- [18] Miller DR, Akbar SA, Morris PA (2014) Nanoscale metal oxide-based heterojunctions for gas sensing: a review. *Sens Actuators B: Chem* 204:250–272
- [19] Lupan O, Postica V, Hoppe M, Wolff N, Polonskyi O, Pauporte T, Viana B, Majerus O, Kienle L, Faupel F, Adelung R (2018) PdO/PdO₂ functionalized ZnO: Pd films for lower operating temperature H₂ gas sensing. *Nanoscale* 10:14107–14127
- [20] Qiu HW, Wang MQ, Li L, Li JJ, Cao MH (2018) Hierarchical MoS₂-microspheres decorated with 3D AuNPs arrays for high-efficiency SERS sensing. *Sens Actuators, B* 255:1407–1414
- [21] Dong C, Jiang M, Tao Y, Shen Y, Lu Y, Yuan Y, Wang Y (2018) Nonaqueous synthesis of Pd-functionalized SnO₂/In₂O₃ nanocomposites for excellent butane sensing properties. *Sens Actuators B: Chem* 257:419–426
- [22] Dong C, Liu X, Han B, Deng S, Xiao X, Wang Y (2016) Nonaqueous synthesis of Ag-functionalized In₂O₃/ZnO nanocomposites for highly sensitive formaldehyde sensor. *Sens Actuators B: Chem* 224:193–200
- [23] Ma J, Fan H, Tian H, Ren X, Wang C, Gao S, Wang W (2018) Ultrahigh sensitivity and selectivity chlorine gas sensing of In₂O₃ hollow microtubules by bio-template method with degreasing cotton. *Sens Actuators B: Chem* 262:17–25
- [24] Wang Z, Hou C, De Q, Gu F, Han D (2018) One-step synthesis of co-doped In₂O₃ nanorods for high response of

- formaldehyde sensor at low temperature. *ACS Sens* 3:468–475
- [25] Liang X, Kim TH, Yoon JW, Kwak CH, Lee JH (2015) Ultrasensitive and ultraspecific detection of H₂S using electrospun CuO-loaded In₂O₃ nanofiber sensors assisted by pulse heating. *Sens Actuators B: Chem* 209:934–942
- [26] Cheng JP, Wang J, Li QQ, Liu HG, Li Y (2016) A review of recent developments in tin dioxide composites for gas sensing application. *J Ind Eng Chem* 44:1–22
- [27] Zhang FH, Wang YC, Wang L, Liu J, Ge HL, Wang B, Huang XY, Wang XD, Chi ZT, Xie WF (2019) High performance In₂(MoO₄)₃@In₂O₃ nanocomposites gas sensor with long-term stability. *J Alloys Compd* 805:180–188
- [28] Zhang W, Zhang W, Chen B, Shao R, Guan R, Zhang W, Zhang Q, Hou G, Yue L (2017) Controllable biomolecule-assisted synthesis and gas sensing properties of In₂O₃ micro/nanostructures with double phases. *Sens Actuators B: Chem* 239:270–278
- [29] Garcia-Marquez A, Glatzel S, Kraupner A, Kiefer K, Siemensmeyer K, Giordano C (2018) Branch-like iron nitride and carbide magnetic fibres using an electrospinning technique. *Chem Eur J* 24:895–4901
- [30] Wu CH, Chou TL, Wu RJ (2018) Rapid detection of trace ozone in TiO₂-In₂O₃ materials by using the differential method. *Sens Actuators B: Chem* 255:117–124
- [31] Hu J, Zou C, Su YJ, Li M, Yang Z, Ge MY, Zhang YF (2017) One-step synthesis of 2D C₃N₄-tin oxide gas sensors for enhanced acetone vapor detection. *Sens Actuators, B* 253:641–651
- [32] Liu BT, Wu CR, Chen G, Chen WB, Peng LL, Yao YC, Wei Z, Zhu H, Han T, Tang DY, Zhou M (2019) All-in-one surface engineering strategy on nickel phosphide arrays towards a robust electrocatalyst for hydrogen evolution reaction. *J Power Sources* 429:46–54
- [33] Liu BT, Wang SW, Mo QH, Peng LL, Cao SX, Wang J, Wu CR, Li C, Guo J, Liu BQ, Chen WB, Lin Y (2018) Epitaxial MoS₂ nanosheets on nitrogen doped graphite foam as a 3D electrode for highly efficient electrochemical hydrogen evolution. *Electrochim Acta* 292:407–418
- [34] Wu CR, Liu BT, Wang J, Su YY, Yan HQ, Ng CT, Li C, Wei JM (2018) 3D structured Mo-doped Ni₃S₂ nanosheets as efficient dual-electrocatalyst for overall water splitting. *Appl Surf Sci* 441:1024–1033
- [35] Zhang J, Zhu Y, Sun JP, Shao MW (2015) Visible-light-enhanced gas sensing of CdS_xSe_{1-x} nanoribbons for acetic acid at room temperature. *Sens Actuators B: Chem* 215:497–503
- [36] Souissi R, Labidi A (2018) Ethanol sensing properties of sprayed B-In₂S₃ thin films. *Sens Actuators B: Chem* 261:522–530
- [37] Hu J, Su YJ, Li M, Yang Z, Ge MY, Zhang YF (2017) One-step synthesis of 2D C₃N₄-tin oxide gas sensors for enhanced acetone vapour detection. *Sens Actuators, B* 253:641–651
- [38] Hu J, Su YJ, Li M, Ye XZ, Cai BF, Kong EW, Yang Z, Zhang YF (2018) Light-assisted recovery for a highly-sensitive NO₂ sensor based on RGO-CeO₂ hybrids. *Sens Actuators, B* 270:119–129
- [39] Wang T, Hu NT, Hu J, Huang D, Jiang WK, Wang S, Wu SM, Zhang YF, Yang Z (2018) Microwave preparation and remarkable ethanol sensing properties of ZnO particles with controlled morphologies in water-ethylene glycol binary solvent system. *Sens Actuators, B* 255:1006–1014
- [40] Wang D, Wan KC, Zhang ML, Li HJ, Wang P, Wang XY, Yang JH (2019) Constructing hierarchical SnO₂ nanofiber/nanosheets for efficient formaldehyde detection. *Sens Actuators B: Chem* 283:714–723
- [41] Zhou TT, Zhang T, Zeng Y, Zhang R, Lou Z, Deng JA, Wang LL (2018) Structure-driven efficient NiFe₂O₄ materials for ultra-fast response electronic sensing platform. *Sens Actuators B: Chem* 255:1436–1444
- [42] Xu K, Tian S, Zhu J, Yang Y, Shi J, Yu T, Yuan C (2018) High selectivity of sulfur-doped SnO₂ in NO₂ detection at lower operating temperatures. *Nanoscale* 10:20761–20771

Publisher's Note Springer Nature remains neutral with regard to jurisdictional claims in published maps and institutional affiliations.